Atmospheric Modeling for Estimating Wind Potential: a Spatio-Temporal Assessment of the Northeast Region of Brazil

Beatriz Rogers Paranhos[1*], Luiz Landau[2], Marcio Cataldi[3]

[1]*Federal Universityof Rio de Janeiro, Alberto Luiz Coimbra Institute for GraduateStudiesandResearch in Engineering, LaboratoryofComputationalMethods in Engineering (LAMCE), Rio de Janeiro Technology Park, Rua Sydney Martins Gomes dos Santos, 179 - Cidade Universitária, 21941-859, Rio de Janeiro, RJ, Brazil, ORCID:0000-0001-6487-3204*

[2]*Federal Universityof Rio de Janeiro, Alberto Luiz Coimbra Institute for GraduateStudiesandResearch in Engineering, LaboratoryofComputationalMethods in Engineering (LAMCE), Rio de Janeiro Technology Park, Rua Sydney Martins Gomes dos Santos, 179 - Cidade Universitária, 21941-859, Rio de Janeiro, RJ, Brazil, ORCID: 0000-0001-7857-9946*

[3]*Fluminense Federal University, Technological Center, SchoolofEngineering, Rua Passo da Pátria, 156 - Bloco D, sala 133, 24210-240, Niterói, RJ, Brazil, ORCID: 0000-0001-9769-0105*

ABSTRACT. This work examines, on different aspects, the sensitivity of the Weather Research and Forecasting (WRF) atmospheric model over the Northeast Region of Brazil to evaluate its performance in representing wind speed and direction. Thus, it seeks to stimulate the growth of the wind industry in the country and the improvement of the WRF. For that, three compositions of physical parameterizations are proposed, two focused on the comparison of the Planetary Boundary Layer (PBL) scheme used and one on the global model Global Forecast System (GFS), as well as verified its results in two horizontal resolutions, 3 and 9 km. The first two weeks of March and September 2018 are evaluated. The applied statistical analyzes are validated through observations provided by the National Institute of Meteorology (INMET), as well as by GFS analyzes. The results demonstrate that the YSU-PBL scheme, with the topo_wind option activated, provided, for the periods of study, the most reliable wind reproduction over the Northeast, as well as the arrangement based on the GFS parameterizations. The WRF presents a better performance, when compared to the other analyzed regions, above all, on the northeastern coast, a range of relevant wind potential and, therefore, of great applicability of the model.

1. INTRODUCTION

The global search for trying to stop the climate crisis that is happening on the planet is perceptible through mechanisms such as the Paris Agreement, carried out during the 21st Conference of the Parties (COP 21) in 2015. With the participation of Brazil, this treaty wishes maintain, in relation to pre-industrial levels, the growth of the global average temperature below 2.0º C, through measures that reduce the emission of greenhouse gases [1, 2]. According to Arantegui and Jäger-Waldau [1], approximately 65% of the world's emissions of CO2, a long-lived greenhouse gas, come from the combustion of fossil fuels. Thus, many investments have been made with a focus on the decarbonization of energy sources, one of its main niches being the use and development of wind energy. For example, Hernández et al. [3] estimate that wind energy is capable of reducing total emissions of

carbon dioxide in the European Union from approximately 6.600 to 13.100 Mt, depending on the technology involved, between 2015 and 2050.

In 2019, the total installed capacity of wind generation in the world was 650,758 MW. This is reflected in a growth of around 104%, when compared to 2013, and of about 33%, in relation to 2016 [4]. Such expansion of the sector is also observed in the Brazilian territory. According to EPE [5], in 2019, in the country, electrical production from wind energy was 55.986 GWh, which translates into an increase of approximately 15.5% when compared to the previous year. The Northeast Region is, in Brazil, the one that most develops in this branch, having generated, in 2019, about 89% of the electricity coming from this source. In order to minimize uncertainties in the wind estimate, which undermines the country's energy security and the expansion of the wind industry, it is

necessary to use efficient mechanisms for its forecast. In this sense, the WRF presents itself as one of the most widely used atmospheric models worldwide, with wide possibilities for evolution [6]. Although it is a promising tool for gauging wind data, considering the physical phenomena acting on a given surface and reducing the dependence on instrumental apparatus for in situ measurements, authors such as Carvalho et al. [7], Draxl et al. [8] and Santos-Alamillos et al. [9], demonstrate that the WRF's performance varies depending on specific factors of the simulation area in question. Therefore, sensitivity analyzes of the model have been carried out in different parts of the planet, in order to find better possibilities of local wind forecasts compared to the alternatives offered by the WRF and favoring the development of the model. This is the case of the work by Avolio et al. [10] that, among 5 evaluated WRF Planetary Boundary Layer schemes applied in the region of Calabria, Italy, found that ACM2 and YSU obtained the most satisfactory performances both in terms of wind speed and direction, when considering the vertical profile of the wind. The study by Carvalho et al. [7] compared 5 WRF PBL schemes over the Iberian Peninsula, noting that the most suitable performance for wind data simulation and for wind production estimates was ACM2. Thus, the present study aims to analyze the sensitivity of the WRF model, with regard to its wind speed and direction results, over the Northeast Region of Brazil, seeking to reduce associated errors and, thus, favor the operational planning of wind parks and the management of the distribution of the generated energy, as well as encouraging the growth of this sector in the country, the improvement of the WRF in this area of the map and providing support for new scientific research. For this, in this work it is evaluated, through high performance modeling, which physical parameterizations, among three different arrangements, lead to a more satisfactory local representation of the wind, using two horizontal resolutions, at two different times of the year. In addition, we find out at which points in the northeastern territory the WRF provides the most appropriate wind performance and which areas are most vulnerable to low quality reproductions.

In addition, in order to verify the degree of influence of the input data used and their treatment, the results of the WRF are compared to those referring to the analysis of the GFS model, applied as an initial and boundary condition in the simulations. This article is organized as follows: Section 2 gathers the materials and methods used, detailing the study area, the choice of data to validate the results, the adjustment of the WRF and the characteristics of the simulations, as well as the use of the GFS and the statistics selected for evaluation. Section 3 presents the results and the associated discussions. Section 4 makes the final considerations and concludes the work.

2. MATERIALS AND METHODS

2.1 Study area and selection of observed data

The Northeast Region of Brazil is composed of the States of Maranhão (MA), Piauí (PI), Ceará (CE), Rio Grande do Norte (RN), Paraíba (PB), Pernambuco (PE), Alagoas (AL), Sergipe (SE) and Bahia (BA). Its territory extends for more than 1.5 million km2, being the Region that shelters the largest coast of the country, with more than 3 thousand km of dimension [11]. The Northeast has a large share in the generation of Brazilian wind energy [5]. Because of this, the present work sought to concentrate its study area in the zone that encompasses the main northeastern wind farms, aiming to assist the different users of wind data for better decision making, as well as to favor the analysis of localities for future wind use [12]. In order to validate the results of this study, anemometric data from automatic surface observation meteorological stations from the National Institute of Meteorology, measured at a height of 10 m, were selected [13]. In all, 18 stations were elected, 2 in each state in the Northeast Region (Table 1). A satisfactory spatial distribution of the observed data was sought together with its complete hourly availability for the periods of time used.

Despite such an effort, the Aracaú Station (A360), in Ceará, did not present some data for the wind direction of September 2018. Therefore, its validation of the direction in that month was discarded, only performing such procedure for the wind speed.

2.2 Adjusting the WRF and characterizing the simulations

The sensitivity tests were performed considering version 4.0.3 of the Advanced Research WRF (ARW-WRF), developed by the National Center for Atmospheric Research (NCAR). So that a high performance modeling was computationally executable, this work relied on the use of the supercomputer Lobo Carneiro, from the Alberto Luiz Coimbra Institute for Graduate Studies and Research in Engineering (COPPE), at the Federal University of Rio de Janeiro (UFRJ). In adjusting the WRF, two domains were used (Figure 1), whose nesting occurred with the exchange of information in one-way. The first one, d01, with a horizontal resolution of 9 km, was dimensioned at 3,600 km x 3,600 km. The second, d02, refers to the study area, with dimensions of 1,425 km x 1,425 km and horizontal grid spacing of 3 km. The central point of the two grids is located in the southeast of the State of Ceará, at -7.02 latitude and -39.29 longitude. In order to smooth cartographic distortions on the study area, located near the Equator, the projection selected was that of Mercator [14].

Table 1 Selected Weather Stations and their main characteristics

State	City	Station code	Detainer	Latitude (⁰)	Longitude (⁰)	Altitude (m)
Alagoas	Maceió	A303	INMET	-9.55	-35.77	84
	Palmeira dos Índios	A327	INMET	-9.42	-36.62	278
Bahia	Lençóis	A425	INMET	-12.56	-41.39	438
	Uauá	A435	INMET	-9.83	-39.50	451
Ceará	Aracaú	A360	INMET	-3.12	-40.09	67
	Jaguaribe	A358	INMET	-5.91	-38.63	149
Maranhão	Bacabal	A220	INMET	-4.24	-44.79	22
	Farol Santana	A217	INMET	-2.27	-43.62	10
Paraíba	Campina Grande	A313	INMET	-7.23	-35.90	546
	Patos	A321	INMET	-7.08	-37.27	264
Pernambuco	Arco verde	A309	INMET	-8.43	-37.06	684
	Serra Talhada	A350	INMET	-7.95	-38.30	499
Piauí	Caracol	A337	INMET	-9.29	-43.32	515
	Picos	A343	INMET	-7.07	-41.40	233
Rio Grande do Norte	Mossoró	A318	INMET	-4.90	-37.37	29
	Natal	A304	INMET	-5.84	-35.21	47
Sergipe	Aracajú	A409	INMET	-10.95	-37.05	4
	Poço Verde	A419	INMET	-10.74	-38.11	367
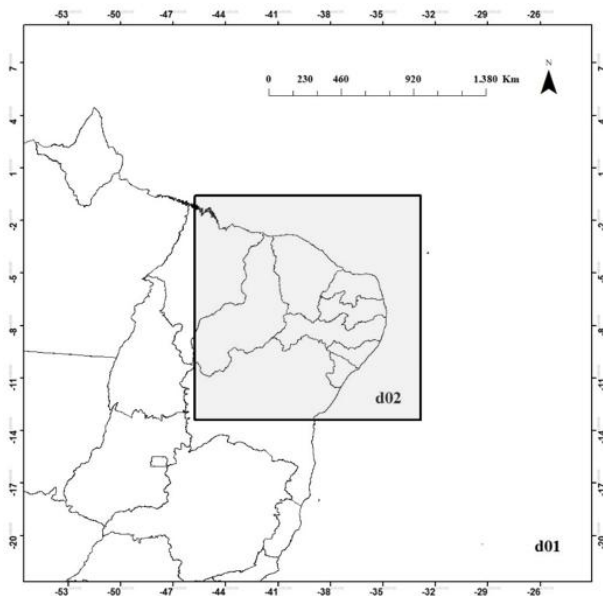
Fig. 1. Layout of the grids used in the WRF simulations

The initial and boundary conditions were obtained from the National Centers for Environmental Prediction (NCEP), through the analysis of the global GFS model, provided every 6 hours, with a horizontal resolution of 0.25o. Topography and land use data came from the Moderate Resolution Imaging Spectroradiometer (MODIS), configured at a resolution of 30 arc seconds for both grids.

The vertical resolution of the WRF was set at 45 vertical levels, with 12 of these levels less than 500 m from the surface. In order to soften the orographic effects on the surface coordinates, and, consequently, to avoid numerical errors, the hybrid coordinate system was used [15]. In order to carry out the simulations, in 2018, the first half of March was selected, a month typically with high rainfall levels in the Northeast Region and low wind intensities. In addition, the first fifteen days of September 2018 were chosen, as it is a time of low rainfall and high wind intensity in this extension of the Brazilian territory [16, 17].

The simulations were divided into one initialization and two more reinitializations for each of the evaluated fortnights, seeking to reduce numerical errors in the representation of the wind [18, 19]. In each execution, the first 6 h of simulation were discarded, considered time for model adjustment (spin up) so that the WRF would achieve computational stability [20].The time intervals that make up each of the simulations of March and September 2018 are shown in Table 2 and Table 3, respectively. It is worth mentioning that the file of initial conditions and contour of February 28, 2018, from 18h UTC, was damaged, being neglected. Soon, the March simulations started at 00h UTC on the 1st.

Table 2 Time intervals of the March 2018 simulations

Start	End
00h UTC 03/01/2018	06h UTC 03/06/2018
00h UTC 03/06/2018	06h UTC 03/11/2018
00h UTC 03/11/2018	06h UTC 03/16/2018

Table 3 Time intervals of the September 2018 simulations

Start	End
18h UTC 08/31/2018	00h UTC 09/06/2018
18h UTC 09/05/2018	00h UTC 09/11/2018
18h UTC 09/10/2018	00h UTC 09/16/2018

Three different arrangements were selected for physical parameterizations, called configuration 1 (C1), configuration 2 (C2) and configuration 3 (C3), gathered in Table 4, Table 5 and Table 6, in that order. The first two are differentiated by the Planetary Limit Layer scheme adopted, with the Microphysics, Long Wave Radiation, Short Wave Radiation, Surface Layer, Earth Surface Model and Cumulus schemes being fixed. The PBL options employed were the Yonsei University Scheme (YSU), in C1, and the Asymmetric Convection Model 2 Scheme (ACM2), in C2 [21, 22]. It is noteworthy that, in all cases, the Cumulus parameterization was only activated for the 9 km grid [23, 24].

Table 4 Physical parameterizations used in the C1 configuration

Physical process	Scheme	References
Microphysics	WSM6	[30]
Long wave radiation	RRTMG	[31]
Short wave radiation	RRTMG	[31]
Surface Layer	Revised MM5 Monin-Obukhov + topo_wind	[25, 32]
Land surface model	Unified Noah *Land-Surface Model*	[33]
Planetary boundary layer	YSU	[21]
Cumulus	Kain-Fritsch	[34]

Along with the parameterization of the Surface Layer, in C1, the Topographic Correction for Surface Winds to Represent Extra Drag from Sub – grid Topography and Enhanced Flow at Hill Tops (topo_wind) option 1 (Jiménez method) was included. It works only coupled to

YSU and its main objective is to reproduce the orographic effects on surface circulations on a sub-grid scale [25]. In turn, for the composition of C3, physical parameterizations inspired by those used by the global GFS model were chosen. It is noteworthy that the MYNN 2.5 options were activated for the mass flow scheme (bl_mynn_edmf = 1), the movement quantity transport scheme (bl_mynn_edmf_mom = 1) and the Turbulent Kinetic Energy transport scheme - TKE (bl_mynn_edmf_tke = 1) [26, 27, 28, 29].

Table 5 Physical parameterizations used in the C2 configuration

Physical process	Scheme	References
Microphysics	WSM6	[30]
Long wave radiation	RRTMG	[31]
Short wave radiation	RRTMG	[31]
Surface Layer	Revised MM5 Monin-Obukhov	[32]
Land surface model	Unified Noah *Land-Surface Model*	[33]
Planetary boundary layer	ACM2	[22]
Cumulus	Kain-Fritsch	[34]

Table 6 Physical parameterizations used in the C3 configuration

Physical process	Scheme	References
Microphysics	Eta Ferrier	[35]
Long wave radiation	RRTMG	[31]
Short wave radiation	RRMTG	[31]
Surface Layer	MYNN	
Land surface model	Unified Noah *Land-Surface Model*	[33]
Planetary boundary layer	MYNN 2.5	[36, 37, 38]
Cumulus	New Simplified Arakawa–Schubert Scheme (for Basic WRF)	[39, 40]

2.3 Using GFS

From the GFS analysis data used as the initial and boundary condition in the WRF simulations, for the same periods, the performances of the global model were also directly evaluated. Thus, the GFS analyzes served as another way to validate the results of the WRF simulations.

In addition, the comparison between wind speed and direction provided by WRF and GFS analyzes helps to ascertain the sensitivity of the first model, considering whether the greatest impact on performance comes from the selection of physical parameterizations or from the initial and contour conditions themselves employed.

2.4 Applied statistics

Different statistical metrics were used to verify the accuracy of the WRF results, with the 3 and 9 km resolution grids, and the GFS analyzes. The calculations were performed with the hourly results provided by the WRF every 6 h, so that they could be compared to the GFS analyzes.

For the wind speed, the Bias, the Root Mean Squared Error (RMSE) and the Correlation Coefficient (r) were used, according to equations (1), (2) and (3), respectively [10, 41, 42].

Bias was applied to measure the model's tendency to overestimate or underestimate its results in relation to reality. The RMSE, in turn, reflects the average magnitude of the error regardless of the signal. Already, the use of r sought to evaluate the ability of the models to monitor the variability of the wind speed, through the linear relationship between the measured data and the observed data [43, 44].

$$Bias = 1/n \sum_{i=1}^{n}(P - O) \qquad (1)$$

$$RMSE = \sqrt{1/n \sum_{i=1}^{n}(P - O)^2} \qquad (2)$$

$$r = \frac{\sum_{i=1}^{n}(P - \bar{P})(O - \bar{O})}{\sqrt{\sum_{i=1}^{n}(P - \bar{P})^2 (O - \bar{O})^2}} \qquad (3)$$

The wind direction was separated into classes, the octants (Table 7), to check whether the WRF simulations and GFS analyzes were able to indicate the correct octant of the direction, or, if not, if one of its neighboring octants was pointed out. Thus, the percentage of errors, in relation to the total sample, in stating the exact octant of the direction, as well as the percentage of relative errors in addition to the octants neighboring to the observed were stipulated.

Modern horizontal-axis wind turbines have orientation mechanisms capable of aligning their rotors and blades according to the wind direction, and it is not essential for this industry to accurately estimate this direction [45].

Table 7 Wind direction octants and their direction intervals

Direction octant	Interval
North	$[0.0^o - 22.5^o]$
Northeast	$[22.5^o - 67.5^o]$
East	$[67.5^o - 112.5^o]$
South east	$[112.5^o - 157.5^o]$
South	$[157.5^o - 202.5^o]$
South west	$[202.5^o - 247.5^o]$
West	$[247.5^o - 292.5^o]$
Northwest	$[292.5^o - 337.5^o]$

3.RESULTS AND DISCUSSION

3.1 Bias

The Bias of the wind speed at 10 m in height, for each of the selected stations, in the first half of March 2018, can be evaluated through Figure 2. In it, the results of each of the proposed WRF configurations are gathered, in the horizontal resolutions of 3 and 9 km, and of the analysis of the GFS.

It can be seen, through the presentation of positive Bias, that the WRF simulations overestimate, in all places and with both domains, the wind speed. GFS analyzes, in general, show the same trend in the period, except in Picos-PI, where they underestimate the speed. Although negative, this Bias is close to zero. In addition, it is possible to observe that, in 10 of the 18 stations, the resolution of 9 km obtains average errors lower than that of 3 km.

Figure 3 shows the Bias of the wind speed at 10 m for the first fifteen days of September 2018. In this period, it is noted, due to its positive values, that there is again an overestimation of the wind speed in relation to the data observed with all the simulated WRF options and everywhere. The GFS analyzes underestimate the speed in Maceió - AL and in Arco Verde - PE. Contrary to what was observed in March 13 of the 18 points achieved superior performances with the 3 km grid with at least one of the WRF configurations.

Authors such as Carvalho et al. [46] and Avolio et al. [10], among others, had already demonstrated the WRF's propensity to overestimate wind speed. The first group, found, in Portugal, that this trend is due to the smoothing and simplification of the representation of the terrain by the model. While the second group observed a similar pattern in southern Italy.
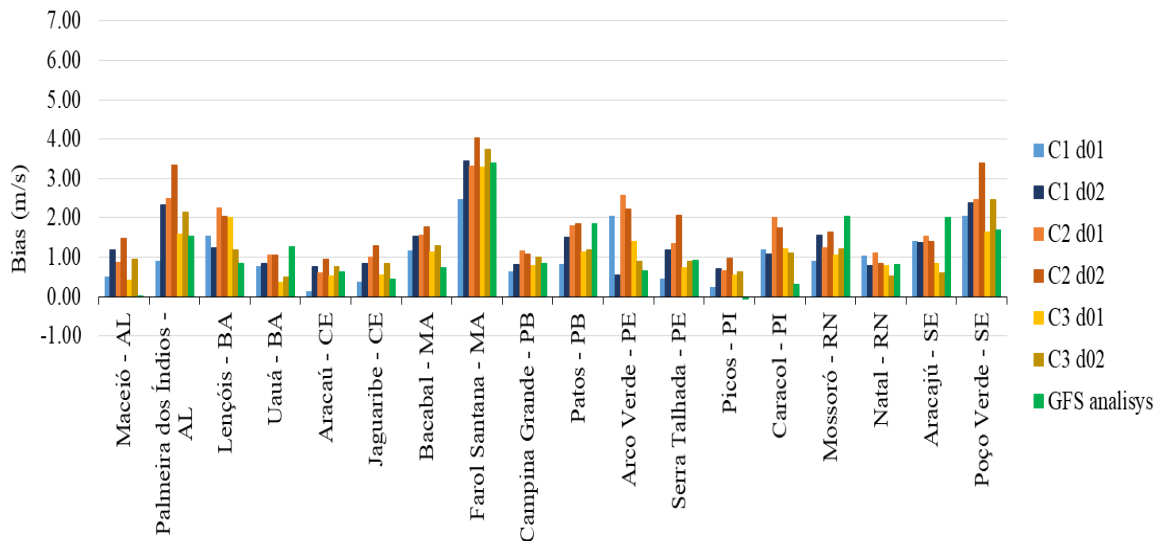
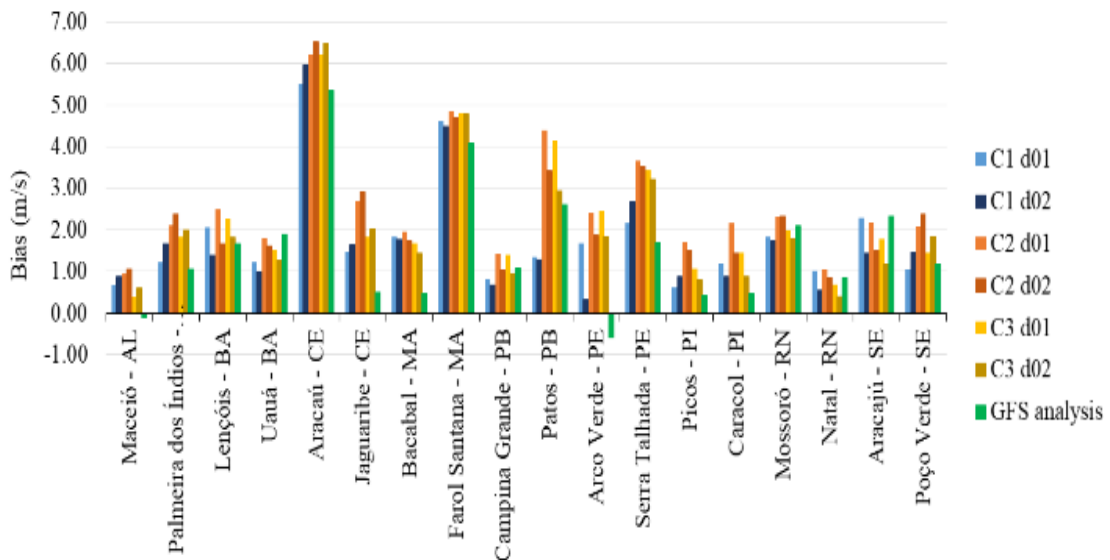**Fig. 2.** Average errors (Bias) of wind speed at 10 m high - first half of March 2018

Fig. 3. Average errors (Bias) of wind speed at 10 m high - first half of September 2018

### 3.2 Spatial distribution of applied statistics

Figure 4 represents the spatial distribution of the lowest values of the RMSE, in (a) and (b), and of the highest r, in (c) and (d). Figure 5 gathers the lowest percentages of the indication of the wrong direction octant, in (a) and (b), and the lowest percentages of error in addition to the octants neighboring the correct one, in (c) and (d). The images on the left (a) and (c), in the two figures, refer to the interval of fifteen days in March and those on the right, (b) and (d), referring to the fifteen days of September 2018.
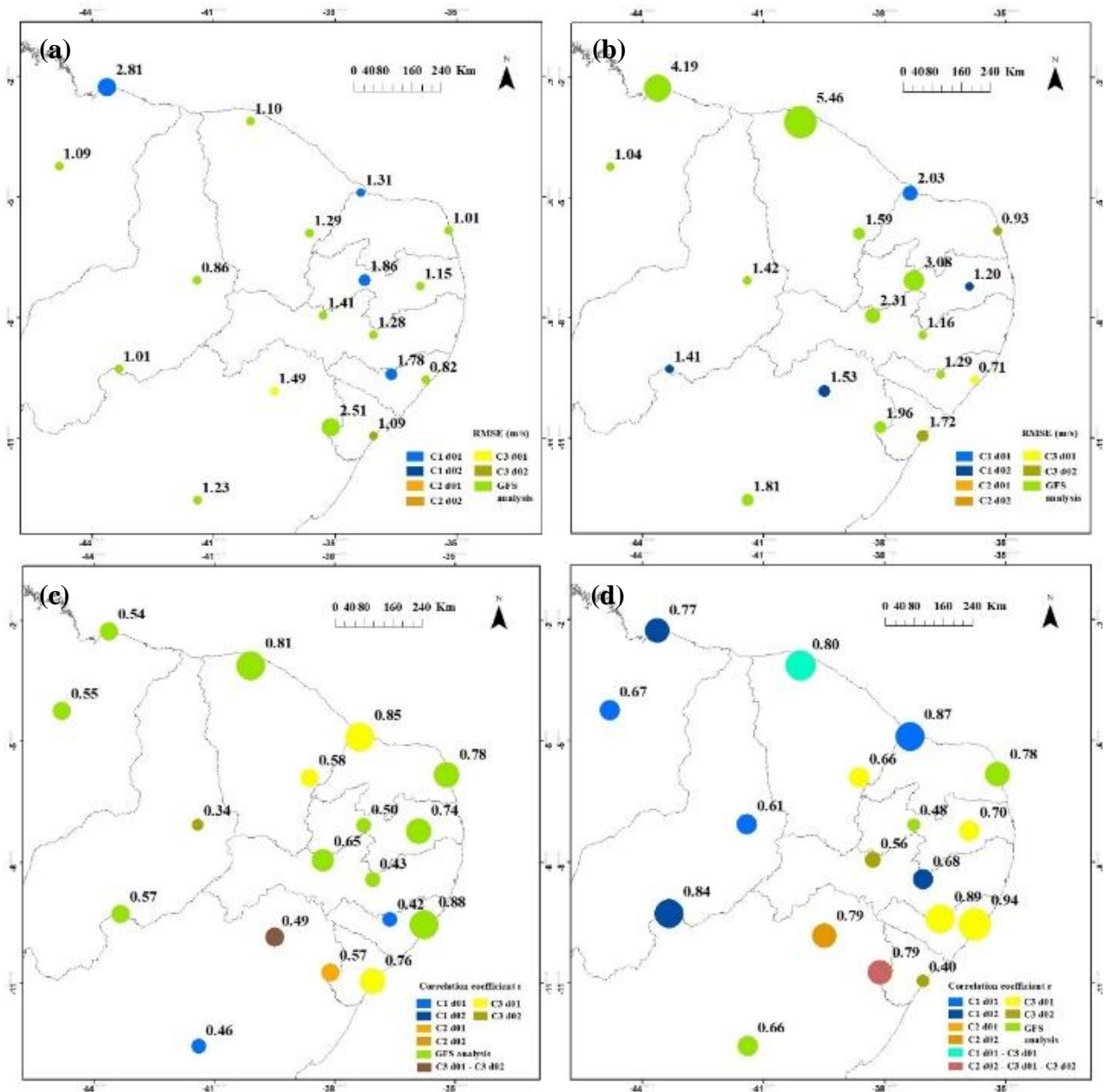
Fig. 4. Spatial distribution of the smallest errors in wind speed at 10 m in height: (a) RMSE for the first half of March 2018; (b) RMSE for the first half of September 2018; (c) r for the first half of March 2018; (d) r for the first half of September 2018
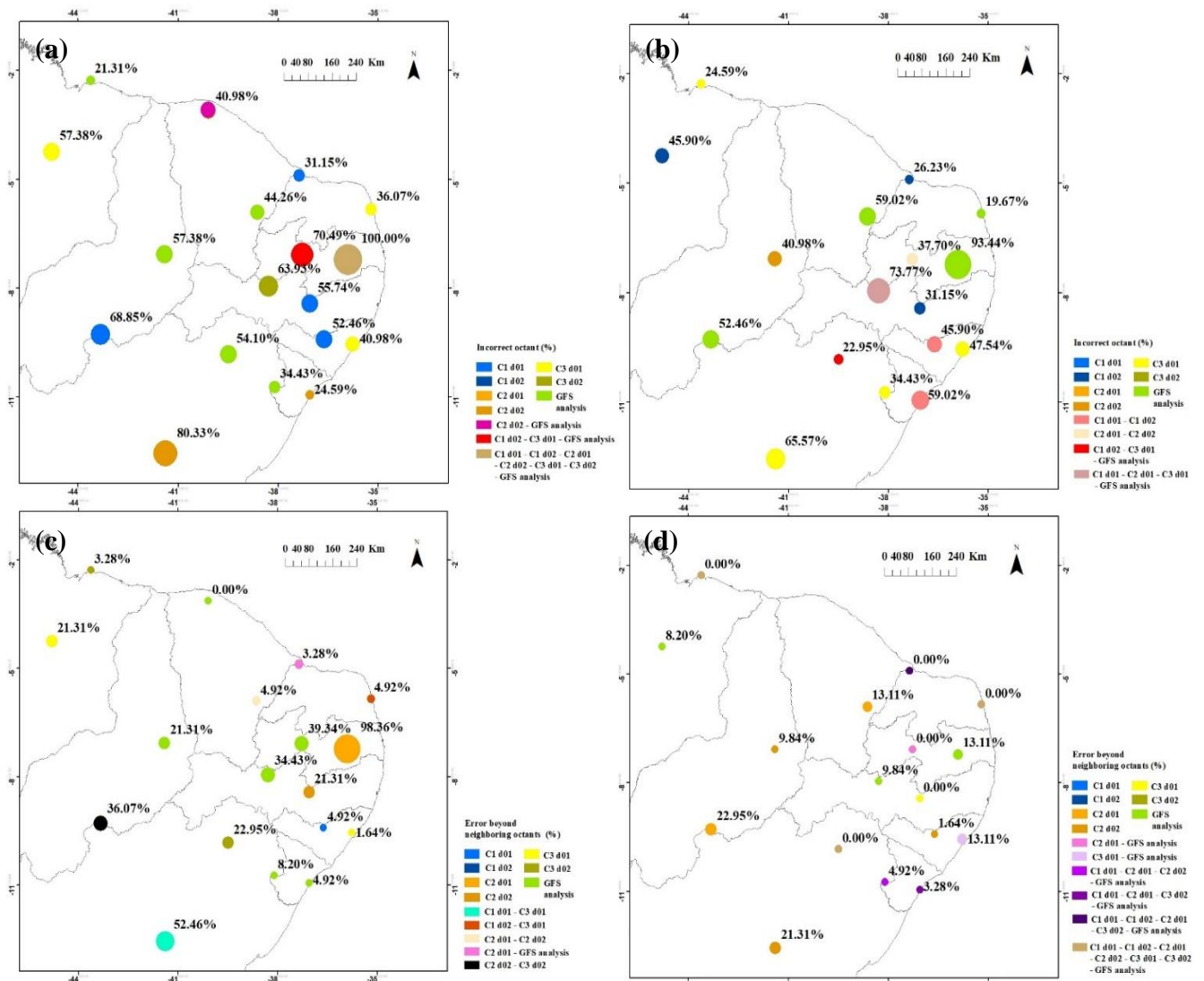
Fig. 5. Spatial distribution of the smallest errors in the wind direction at 10 m in height: (a) RMSE for the first half of March 2018; (b) RMSE for the first half of September 2018; (c) r for the first half of March 2018; (d) r for the first half of September 2018

It can be seen, through the analysis of Figure 4, that the magnitude of the error on the wind speed is predominantly lower, on the territory, with the analyzes of the GFS, both in March and in September. The lower horizontal resolution of GFS analyzes can influence the smallest errors in this magnitude, overestimating this speed with less intensity. As it is a systematic error, it can be corrected, for example, statistically in its post-processing [47].

In March, the WRF simulation that has the largest number of smaller RMSE on the map is the one that uses C1 in the 9 km resolution, all at points that the simulations in general had more difficulty to represent. On the other hand, C3-based reproduction obtained the smallest errors at two points close to each other, north of Bahia, with 9 km of resolution, and on the coast of Sergipe, with 3 km of resolution. In the first half of September, C1 is also the WRF option with the highest frequency of minor errors,

after GFS analyzes. However, this occurs mostly with the 3 km grid. The simulations with C3 have better results at three points, all on the east coast, also with emphasis on the daughter grid. Representations with C2 do not achieve the best performance in any of the evaluation points and intervals.

From the point of view of the linear correlation of wind speed, in March, the GFS analyzes have the best results in most of the map. The application of configuration 3, especially in the resolution of 9 km, is the one that reaches a greater extension of the study area with the highest values of r.

Differently, in September, it is the WRF simulations that predominate with the strongest correlations. Basically, options C1 and C3 obtain the best correlations, with this configuration having one more station of advantage than

8

that. In both cases, the highest frequency of strong correlations occurs with the 9 km grid.

Despite the increase in the error on the magnitude of the wind speed from March to September, there is an increase in the Correlation Coefficient from one period to the next over the entire length of the territory. The accurate estimate of the variability of the wind over time is substantial for the quality of the energy produced and its adequate planning, being, therefore, a relevant aspect that the WRF is able to offer strong correlations.

Through Figure 5, it is noted that, in March 2018, there is heterogeneity between the options that reach the lowest percentage of wrong octants of the wind direction at 10 m high. Nevertheless, GFS analyzes still stand out on the study area, either in isolation or in conjunction with some WRF simulation. Then, the reproductions of C1 and C3 obtain the same number of points with the smallest errors, with an emphasis on the resolution of 9 km.

In the case of the first half of September 2018, once again a heterogeneous distribution of the alternatives with the lowest percentages of error is observed. During this period, GFS analyzes and WRF simulations using C3, with the 9 km grid, are tied with the greatest number of locations where they achieve superior performance. As for the smallest errors in addition to the octant neighbours to the correct one, in March, a greater presence of the different WRF simulation options on the map is noted. In addition, reproductions with C3 match the GFS analysis and achieve the best performance in this regard, with the 9 km grid appearing and a location more than that of 3 km

In September 2018, a large part of the points generated errors in addition to the neighbouring octants below 10%. In the meantime, there are many places where this occurs with more than one alternative. The simulations associated with configuration 2 are the ones with the best performance, with the 9 km grid taking advantage of two locations in relation to the 3 km. It is worth highlighting the tendency of decreasing the percentage of errors in the wind direction, at 10 m height, from March to September 2018. Furthermore, the aptitude of both WRF simulations and GFS analyzes is demonstrated when, when they do not get it right the octant of the direction, point one of the neighbours to the correct one.

The GFS analyzes were expected to show more representative results of the wind, over the Northeast Region, for all statistical investigations. This is because these analyzes contain observed data assimilated throughout its domain, whereas the WRF had its contact with these observations limited to the initial and boundary conditions.

This oscillation in the WRF's ability to perform better or worse than the GFS analyzes reflects the impact, in the results, of both the input and contour information in the model and the appropriate choice of physical parameterizations for the desired location. The different maps indicate that the Northeast coast tends to have the results closest to reality, both for speed and wind direction. The highlight is on the east coast, an area

of significant wind power generation capacity [48]. The north coast, especially on the coast of Maranhão and Ceará, despite good reliability for the linear correlation and for determining the direction octant, has low accuracy for the magnitude of the wind speed error. The area that, predominantly, presented the worst statistical performances of wind speed and direction, at 10 m in height, was that which covers the interior of Paraíba and Pernambuco, as well as Lençóis, located in the most central part of Bahia.

Note that Campina Grande behaved as an outlier within the sample, with errors in the indication of the wind direction above 90% when applying all WRF options, as well as with the GFS analyzes. It was only in the period of September 2018 that the error, besides the neighboring octants, in this place, managed to fall to less than 15%.

The performance of atmospheric systems over the Northeast Region may influence the similar behavior between the WRF simulations and the GFS analyzes on the map. The interior of Paraíba and Pernambuco is influenced by the Intertropical Convergence Zone (ZCIT) and also suffers the impacts of moisture transport from the ocean to the continent, being characterized as a place of formation of Lines of Instability and that can be covered by precipitation induced by Upper Tropospheric Cyclonic Vortex (UTCV) [49,50].

The central area of Bahia, on the other hand, is mainly affected by cold fronts and the formation of a UTCV. The South Atlantic Subtropical Anticyclone (SASA) is also able to impact this portion of the map thanks to the displacement of moisture inland [49, 50]. Otherwise, the northeastern coast, starting from Rio Grande do Norte and ending in Sergipe, suffers interference from trade winds and breeze circulation, in addition to SASA, favoring the intensification and stability of the wind [49, 50].

Thus, there is an association between areas of greater susceptibility to cloud formation with a worse performance in wind simulations by WRF. The occurrence of precipitation tends to weaken the intensity of the winds in the Northeast, which, in turn, generates greater vulnerability of the model to errors [17]. In addition, in March 2018, a La Niña ended [51]. According to Santos e Silva [17], this phenomenon is also responsible for contributing to the decrease in wind intensity in the Northeast Region of Brazil.

3.3 Topographic analysis

In order to complement the spatio-temporal analyzes, a map was created representing the altimetric difference between the dimensions provided by Embrapa's Digital Elevation Model (DEM) [52], with a resolution equivalent to approximately 90 m, and the dimensions applied by WRF to represent the topography of the region, of about 1 km of resolution.

Through Figure 6, there is a predominance of negative differences between the DEM and the topography used by the WRF, indicating the propensity of this model to apply a higher level than the real one. The average of this

altitude difference over the study area is -2 m and its standard deviation is 65 m.

The coastal strip is, in general, able to have a realistic topographic representation within the WRF, as observed by the small altimetric difference in relation to the MDE. This fact reaffirms the quality of the model's performance in estimating wind speed and direction in this region. In contrast, in the interior of Paraíba and Pernambuco, a place of low wind performance in the evaluated periods, the quota differences fluctuate between positive and negative over small distances. A similar situation occurs in Lençóis, Bahia. This variation in the representation of the topography by the WRF may end up intervening in the intensity and direction of the atmospheric flow over these regions, impairing the performance of the simulations [53].

Santos et al. [54] had already observed in Triunfo, interior of Pernambuco, a smoothing of topographic conditions in the WRF in relation to reality. However, the authors reached underestimated results of wind speed, which goes in the opposite direction to that observed in the present work, in which overestimated results were found.
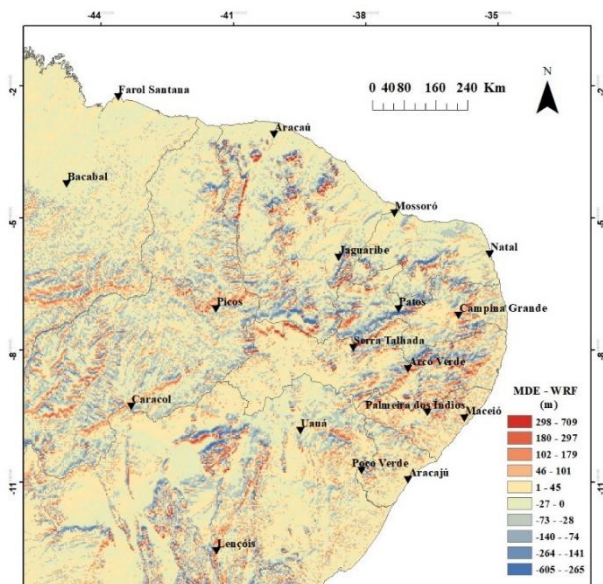
Fig. 6. Altimetric difference between a Digital Elevation Model and the topographic representation of the WRF

4.CONCLUSIONS

This work aimed to analyze, under different spectra, the sensitivity of the WRF atmospheric model in relation to the wind data produced by it over the Northeast Region of Brazil. Therefore, we sought to verify which parameter composition was capable of providing more reliable wind results.

Of the three physical parameterization arrangements investigated, configurations C1 and C3 were, within the studied time intervals, those that presented simulations together with performances more representative of both the speed and the direction of the wind in the different points of the study area.

The C1 configuration consists of the YSU scheme for the Planetary Boundary Layer, with the topo_wind option

enabled. On the other hand, C3 is the GFS-based arrangement, which contains the MYNN 2.5 scheme for the PBL. The other characteristics of C1 and C3 are detailed in section 2.2.

In general, in the evaluated periods, the GFS analyzes showed lower errors regarding the magnitude of the wind intensity, while the WRF simulations achieved greater successes with its ability to express the variability of the wind speed over time and its direction. . As the errors on the magnitude are simpler for statistical correction than the others, the use of WRF showed an advantage in relation to GFS analyzes. The outstanding performance of the WRF simulations on the GFS analyzes was not assumed, since the said analyzes, despite their lower resolution, assimilate data observed in their domain. The WRF, on the other hand, had contact with these data restricted to initial and frontier conditions. In an operational forecast, after using the GFS analysis in the initial conditions, the WRF only has information from the GFS forecast as a boundary condition and from the WRF forecast itself. Spatially examining,it was noted that the most accurate performances, both in the WRF simulations and in the GFS analyzes, tend to be concentrated on the northeastern coast, especially on the east coast, which is a particularly favorable track for wind generation. In other words, the WRF has a promising application for the sector in these locations. Otherwise, the most discrepant wind results in relation to the observations are, above all, in nuclei in the interior of Paraíba and Pernambuco, as well as more in the center of Bahia.

In terms of seasonality, it was noted that in the first half of September the WRF simulations performed better than the same period in March. In addition to being a month often of more intense rainfall and milder wind speeds in the Northeast, in 2018, March passed the end of a La Niña, which may have made the model's representations even more difficult.

In addition, it was found that, in the period of greatest instability and cloudiness, March, simulations that contained a lower grid resolution tended to achieve better performance. In the time of more stable weather, September, a more refined resolution was necessary to reach lower errors on the intensity of the wind and, in the case of variability and direction, this oscillated more evenly according to the season investigated.

The different wind behaviors reproduced by the WRF over the Northeast region are in line with the topographic representation capacity used by the model. The most critical points observed in terms of accuracy tend to be those in which the topography used by the WRF is more coarse, which ends up affecting the air flow simulation.

For future work, it is suggested that sensitivity analyzes be carried out on the Northeast Region, encompassing a wider range of arrangements for physical parameterizations, as well as that simulations be carried out for longer periods of time and for other times of the year.

In addition, it is proposed to add to such evaluations the comparison between simulations that perform the technique of assimilation of observed data and those

without this mechanism activated, to verify the ability to improve or not in the reproduction of the wind in the Northeast.

REFERENCES

[1] Arantegui, R. L.; Jäger-Waldau, A. Photovoltaics and wind status in the European Union after the Paris Agreement. Renewable and Sustainable Energy Reviews, v. 81, p. 2460-2471, 2018.

[2] Hoegh-Guldberg, Ove et al. The human imperative of stabilizing global climate change at 1.5 C. Science, v. 365, n. 6459, 2019.

[3] Hernández, C. V.; González, J. S.; Fernández-Blanco, R. New method to assess the long-term role of wind energy generation in reduction of CO2 emissions – case study of the European union. Journal of cleaner production, v. 207, p. 1099-1111, 2019.

[4] WWEA. Statistics. WWEA/World Wind Energy Association. Available at: https://wwindea.org/blog/category/statistics/. Accessed on 20 nov. 2020.

[5] EPE. BalançoEnergético Nacional 2020: Ano base 2019 (National Energy Balance 2020: Base year 2019). EPE/Energy Research Company. Rio de Janeiro. 2020.

[6] Powers, J. G. et al. The weather research and forecasting model: Overview, system efforts, and future directions. Bulletin of the American Meteorological Society, v. 98, n. 8, p. 1717–1737, 2017.

[7] Carvalho, D. et al. Sensitivity of the WRF model wind simulation and wind energy production estimates to planetary boundary layer parameterizations for onshore and offshore areas in the Iberian Peninsula. Applied Energy, Vol. 135, p. 234–246, 2014.

[8] Draxl, C. et al. Evaluating winds and vertical wind shear from Weather Research and Forecasting model forecasts using seven planetary boundary layer schemes. Wind Energy, v. 17, n. 1, p. 39-55, 2014.

[9] Santos-Alamillos, F. J. et al. Analysis of WRF model wind estimate sensitivity to physics parameterization choice and terrain representation in Andalusia (Southern Spain). Journal of Applied Meteorology and Climatology, v. 52, n. 7, p. 1592–1609, 2013.

[10] Avolio, E. et al. Sensitivity analysis of WRF model PBL schemes in simulating boundary-layer variables in southern Italy: An experimental campaign. Atmospheric Research, v. 192, n. April, p. 58–71, 2017.

[11] Getirana, A.; Libonati, R.; Cataldi, M. Brazil is in water crisis – it needs a drought plan. Nature, v. 600, p. 218-220, 2021.

[12] IBGE. Anuário Estatístico do Brasil (Brazilian Statistical Yearbook). IBGE/ Brazilian Institute of Geography and Statistics. Rio de Janeiro, v.79, p.1-1-8-50, 2020.

[13] Abeeólica. Números Abeeólica – Fevereiro de 2019 (ABEEólica Numbers - February 2019). Abeeólica/Brazilian Wind Energy Association. Available at: http://abeeolica.org.br/dados-abeeolica/. Accessed on 17 jan. 2020.

[14] Inmet. Technical Note no 001/2011/Seger/Laime/Csc/Inmet. Inmet/ National Institute of Meteorology. n. 001, p. 1–11, 2011.

[15] NCAR. WRF-ARW version 4 Modeling System User's Guide. NCAR/National Center For Atmospheric Research. Mesoscale & Microscale Meteorology Division. 2019.

[16] Park, S.-H.; Klemp, J. B.; Kim, J.-H. Hybrid Mass Coordinate in WRF-ARW and Its Impact on Upper-Level Turbulence Forecasting. Monthly Weather Review, Vol. 147, n. 3, p. 971–985, 2019.

[17] Silveira, C. DA S. et al. Seasonality of Precipitation Over the Northern Brazilian Northeast in the Simulations of the IPCC-AR4. Revista Brasileira de Recursos Hídricos (Brazilian Journal of Water Resources), v. 17, n. 3, p. 125–134, 2012.

[18] Santos, A. T. S.; Silva, C. M. S. Seasonality, Interannual Variability, and Linear Tendency of Wind Speeds in the Northeast Brazil from 1986 To 2011. The Scientific World Journal, v. 2013, p. 1–10, 2013.

[19] Qian, J.-H.; Seth, A.; Zebiak, S. Reinitialized versus Continuous Simulations for Regional Climate Downscaling. Monthly Weather Review, Vol. 131, n. 11, p. 2857–2874, 2003.

[20] Lo, J. C. F .; Yang, Z. L.; Pielke, R. A. Assessment of three dynamical climate downscaling methods using the Weather Research and Forecasting (WRF) model. Journal of Geophysical Research Atmospheres, v. 113, n. 9, 2008.

[21] Lucas-Picher, P. et al. Dynamical Downscaling with Reinitializations: A Method to Generate Finescale Climate Datasets Suitable for Impact Studies. Journal of Hydrometeorology, v. 14, n. 4, p. 1159–1174, 2013.

[22] HONG, S.-Y.; Noh, Y.; Dudhia, J. A New Vertical Diffusion Package with an Explicit Treatment of Entrainment Processes. Monthly Weather Review, Vol. 134, n. 9, p. 2318–2341, 2006.

[23] Pleim, J. E. A Combined Local and Nonlocal Closure Model for the Atmospheric Boundary Layer. Part I: Model Description and Testing. Journal of Applied Meteorology and Climatology, v. 46, n. 9, p. 1383–1395, 2007.

[24] De Meij, A.; Vinuesa, J. F.; Maupas, V. Ghi calculation sensitivity on microphysics, land- and cumulus parameterization in WRF over the Reunion Island. Atmospheric Research, v. 204, n. January, p. 12–20, 2018.

[25] Skamarock, W. et al. A description of the advanced research WRF version 4. Technical Report, March, p. 162, 2019.

[26] Jiménez, P. A.; Dudhia, J. Improving the representation of resolved and unresolved topographic effects on surface wind in the wrf model. Journal of Applied Meteorology and Climatology, v. 51, n. 2, p. 300–316, 2012.

[27] DTC. Common Community Physics Package (CCPP) Scientific Documentation Version 3.0. DTC/Developmental Testbed Center. Available at: https://dtcenter.org/GMTB/v3.0/sci_doc/allscheme_page.html. Accessed on 6 jan. 2020.

[28] DTC. GFS Operational Physics Documentation. DTC/Developmental Testbed Center. Available at: https://dtcenter.org/GMTB/gfs_phys_doc_dev/index.html. Accessed on 6 jan. 2020.

[29] NOAA. Global Forecast System - Global Spectral Model (GSM) - v13.0.2. NOAA/National Oceanic and Atmospheric Administration. Available at: https://vlab.ncep.noaa.gov/web/gfs/documentation. Accessed on 6 jan. 2020.

[30] Campana, K. et al. The Development and Success of NCEP's Global Forecast System. In: 99th American Meteorological Society Annual Meeting. AMS, 2019.

[31] Hong, S-Y; Lim, J-O J. The WRF single-moment 6-class microphysics scheme (WSM6). Asia-Pacific Journal of Atmospheric Sciences, v. 42, n. 2, p. 129-151, 2006.

[32] Iacono, M. J. et al. Radiative forcing by long-lived greenhouse gases: Calculations with the AER radiative transfer models. Journal of Geophysical Research Atmospheres, v. 113, n. 13, p. 2–9, 2008.

[33] Jiménez, P. A. et al. A Revised Scheme for the WRF Surface Layer Formulation. Monthly Weather Review, Vol. 140, n. 3, p. 898–918, 2012.

[34] Tewari, M. et al. Implementation and verification of the unified noah land surface model in the WRF model. Bulletin of the American Meteorological Society, p. 2165–2170, 2004.

[35] Kain, J. S. The Kain – Fritsch convective parameterization: an update. Journal of applied meteorology, v. 43, n. 1, p. 170-181, 2004.

[36] Rogers, E. et al. National Oceanic and Atmospheric Administration Changes to the Ncep Meso Eta Analysis and Forecast System: Increase in resolution, new cloud microphysics, modified precipitation assimilation, modified 3DVAR analysis. NWS Tech. Proced. Bull, v. 488, p. 15, 2001.

[37] Nakanishi, M.; Niino, H. Development of an improved turbulence closure model for the atmospheric boundary layer. Journal of the Meteorological Society of Japan, v. 87, n. 5, p. 895–912, 2009.

[38] Nakanishi, M.; Niino, H. An improved Mellor-Yamada Level-3 model: Its numerical stability and application to a regional prediction of advection fog.

Boundary-Layer Meteorology, v. 119, n. 2, p. 397–407, 2006.

[39] Olson, J. B. et al. A description of the Mynn-Edmf scheme and the coupling to other components in WRF – ARW. NOAA Technical Memorandum OAR GSD-61, NOAA. 2019.

[40] Han, J.; Pan, H. L. Revision of convection and vertical diffusion schemes in the Ncep Global Forecast System. Weather and Forecasting, v. 26, n. 4, p. 520–533, 2011.

[41] Kwon, Y. C.; Hong, S. Y. A mass-flux cumulus parameterization scheme across gray-zone resolutions. Monthly Weather Review, Vol. 145, n. 2, p. 583–598, 2017.

[42] Mattar, C.; Borvarán, D. Offshore wind power simulation by using WRF in the central coast of Chile. Renewable Energy, v. 94, p. 22–31, 2016.

[43] Ratjiranukool, P.; Ratjiranukool, S. Evaluating Wind Speed by WRF Model over Northern Thailand. Energy Procedia, v. 138, p. 1171–1176, 2017.

[44] Chai, T; Draxler, R. R. Root mean square error (RMSE) or mean absolute error (MAE)? - Arguments against avoiding RMSE in the literature. Geoscientific model development, v. 7, n. 3, p. 1247-1250, 2014.

[45] Hallak, R.; Pereira Filho, A. J. Methodology for performance analysis of convective system simulations in the metropolitan region of São Paulo with the ARPS model: sensitivity to variations with advection and data assimilation schemes. Revista Brasileira de Meteorologia (Brazilian Journal of Meteorology), v. 26, n. 4, p. 591-608, 2011.

[46] Amaral, B. M. Modelos Varx para Geração de Cenários de Vento e Vazão Aplicados a Comercialização de Energia (VARX Models for Generation of Wind and Flow Scenarios Applied to Energy Trading). Masters dissertation. Pontifical Catholic University of Rio de Janeiro - PUC Rio. Rio de Janeiro. 2011.

[47] Carvalho, D. et al. WRF wind simulation and wind energy production estimates forced by different reanalyses: Comparison with observed data for Portugal. Applied Energy, Vol. 117, p. 116-126, 2014.

[48] Saha, S. Response of the NMC MRF model to systematic-error correction within integration. Monthly weather review, v. 120, n. 2, p. 345-360, 1992.

[49] Cepel. Atlas of the Brazilian Wind Potential: Simulations 2013. Cepel/Electric Energy Research Center. Rio de Janeiro. 2017.

[50] Ferreira, A. G .; Da Silva Mello, N. G. Main atmospheric systems acting on the Northeast region of Brazil and the influence of the Pacific and Atlantic oceans on the region's climate. Brazilian Journal of Climatology, v. 1, n. 1, 2005.

[51] Reboita, M. S. et al. Precipitation regimes in South America: a literature review. Brazilian Journal of Meteorology, v. 25, n. 2, p. 185–204, 2010.

[52] NOAA. Cold & Warm Episodes by Season. NOAA/National Oceanic and Atmospheric Administration. Available at: https://origin.cpc.ncep.noaa.gov/products/analysis_monitoring/ensostuff/ONI_v5.php. Accessed on 28 oct. 2020.

[53] Miranda, E. E. de; (Coord.). Brazil in Relief. Campinas: Embrapa Satellite Monitoring, 2005.

Available at: http://www.relevobr.cnpm.embrapa.br. Accessed on 13 feb. 2019.

[54] Stull, R. B. An introduction to boundary layer meteorology. Atmospheric Sciences Library, Dordrecht: Kluwer, 1988, vol. 1, 1988.

[55] Santos, A. T. S. et al. Assessment of Wind resources in two parts of Northeast Brazil with the use of numerical models. Meteorological Applications, v. 23, n. 4, p. 563-573, 2016.